

Fermi National Accelerator Laboratory

FERMILAB-Conf-89/246-E
[E-741/CDF]

**A Study of Weak Boson Production with $W \rightarrow e\nu$
and $Z \rightarrow ee$ at CDF ***

The CDF Collaboration

presented by

T. Kamon
Texas A&M University
College Station, Texas 77843

December 5, 1989

* To be published in the proceedings of the 8th Topical Workshop on $p\bar{p}$ Collider Physics, Castiglione della Pescaia, Italy, September 1-5, 1989.



For the Proceedings in 8th Topical Workshop on $p\bar{p}$ Collider Physics
Castiglione della Pescaia (ITALY) · September 1-5, 1989

A Study of Weak Boson Production with $W \rightarrow e\nu$ and $Z \rightarrow ee$ at CDF

The CDF Collaboration¹

Presented by T.Kamon

Texas A&M University
College Station, Texas, 77843, USA

Abstract

A study has been made of weak boson production with subsequent decays into electron(s) in $p\bar{p}$ collisions at $\sqrt{s} = 1.8$ TeV using the Collider Detector at Fermilab (CDF) for 1988-89 data. Measurements of the ratio $\sigma_{W\cdot B}(W \rightarrow e\nu)/\sigma_{Z\cdot B}(Z \rightarrow e^+e^-)$ and the transverse momentum distributions of the weak bosons, and of associated jet production, are presented. These measurements are compared with theoretical predictions.

¹The collaboration is listed in Appendix A.

1 INTRODUCTION

The study of weak boson production is of great interest in testing the Standard Model (SM): (A) Detailed studies on the properties of weak bosons provide precise tests of the $SU(2)_L \otimes U(1)_Y$ electroweak gauge theory. (B) A quantitative test of perturbative QCD can be provided in the production of weak bosons in association with hard QCD jets.

A data sample with an integrated luminosity of 4.4 pb^{-1} in $\bar{p}p$ collisions has been accumulated using the Collider Detector at Fermilab (CDF) under the successful operation of the Fermilab Tevatron at $\sqrt{s} = 1.8 \text{ TeV}$ in 1988-89. High statistics of W/Z events from the sample allow us to test the electroweak sector and higher order QCD in a new kinematic regime. A deviation from the standard prediction can then be pursued, *i.e. new physics*.

In this paper we present (A) a measurement of the cross section ratio for $W \rightarrow e \nu$ and $Z \rightarrow e^+e^-$ and (B) a preliminary study on transverse momentum distributions of weak bosons and associated jet production, where the bosons subsequently decay into electron(s).

2 THE CDF EXPERIMENT

2.1 The CDF Detector

The CDF detector is a large magnetic spectrometer and is shown in Fig. 1. Detailed description of the CDF detector can be found elsewhere [1]. Here the features relevant to this data analysis are summarized.

Scintillation counter planes on both sides of the interaction region, called the beam-beam counter (BBC), covering the pseudorapidity region $3.2 < |\eta| < 5.9$ are used in the trigger and also as a monitor of the $\bar{p}p$ luminosity.

Vertex Time Projection Chambers (VTPC's) around the beam pipe are used to determine the event vertex in Z and covers an angular region $|\eta| \lesssim 3$. The Central Tracking Chamber (CTC), which surrounds the VTPC system and is immersed in a 1.412 T axial magnetic field, provides three-dimensional tracking and momentum determination for charged particles in the region $|\eta| \lesssim 1.0$ with a resolution of $\delta p_T/p_T^2 = 0.0011 (\text{GeV}/c)^{-1}$ with a beam constraint fit [2].

The electromagnetic (EM) and hadronic (HAD) calorimeters are arranged in a fine grained projective tower geometry covering the polar angles from 2° to 178° . The calorimeters are organized into three angular regions: the central region ($|\eta| \leq 1.1$), the plug region ($1.1 < |\eta| \leq 2.4$), the forward region ($2.4 < |\eta| \leq 4.2$). A gas proportional chamber (CES) is embedded at a depth of $5.9 X_0$ in the central EM (CEM) calorimeter to give an accurate determination of the shower positions in $r \cdot \phi$ (wire readout) and Z (strip readout) views in the calorimeter.

2.2 The CDF 1988-89 Run

The Fermilab Tevatron has delivered a total of 9 pb^{-1} of the integrated luminosity. The CDF has collected 4.4 pb^{-1} of data which contains $\sim 4,500$ candidates of $W \rightarrow e \nu$ and ~ 350 candidates of $Z \rightarrow e^+ e^-$.

The W and Z events used in this analysis were selected from an event sample with the inclusive central electron trigger, which is a hardware trigger requiring (a) at least one hit by charged particle on each side of BBC system and (b) the presence of at least one electron candidate in the central region with a CEM cluster $E_T \geq 12 \text{ GeV}$, the associated track momentum $p_T \geq 6 \text{ GeV}/c$, and a ratio of HAD-to-EM energy in the cluster ≤ 0.125 .

2.3 The Detector Calibration

The calibration of the detector is significant importance in several analyses: the momentum scale for the CTC, the energy scales for EM and HAD calorimeters. The momentum scale was checked by studying the mass peaks for $K_s^0 \rightarrow \pi^+ \pi^-$, $J/\psi \rightarrow \mu^+ \mu^-$, and $\Upsilon \rightarrow \mu^+ \mu^-$ [2,3]. The energy scale calibration for the CEM calorimeter was performed using E/p technique [2,3], then the scales for the plug and forward EM calorimeters were verified using the Z mass peak for $Z \rightarrow e^+ e^-$, where one of electron is in the central region. The dijet p_T balancing technique provides a verification of the energy scales for all HAD calorimeters [4].

3 PARTON IDENTIFICATION AT CDF

Since the identification of electrons, jets (for gluon and quarks), and neutrinos is required in this analysis, we summarize the features of the identification variables for electron, the identification algorithm and the momentum correction for jet and neutrino.

3.1 Electron Identification

The CDF has a nice performance of the electron identification because of a magnetic detector. There are the different electron identification variables in the central, plug, and forward regions. Those variables are listed below. The cut values of the variables for the electron identification in our analyses can be found in tables in Sections 4 and 5.

3.1.1 Common electron identification variables

The following two variables are common in the central, plug, and forward regions.

- Isolation of EM cluster [5]:

$$I = \frac{\sum E_T(R_c < 0.4) - E_T(\text{cluster})}{E_T(\text{cluster})},$$

where $\sum E_T(R_c < 0.4)$ is the total transverse energy within a cone of radius of 0.4 centered on the cluster and $R_c = \sqrt{(\Delta\eta)^2 + (\Delta\phi)^2}$.

- Energy leakage to HAD calorimeter in EM cluster:

$$\text{HAD/EM} = \frac{E_{\text{HAD}}}{E_{\text{EM}}},$$

where E_{EM} (E_{HAD}) is an observed energy in EM (HAD) calorimeter.

3.1.2 Central electron identification variables

A nice and detailed description of the identification of the central electrons can be found in Ref.[6]. Here the identification variables are listed.

- Ratio of the calorimeter energy to the matched track momentum:

$$E/p$$

- Geometrical matching of the shower measured in the CES with track reconstructed in the CTC:

$$\begin{aligned}\Delta(r \cdot \phi) &= (r \cdot \phi)_{\text{CES}} - (r \cdot \phi)_{\text{CTC}} \\ \Delta Z &= Z_{\text{CES}} - Z_{\text{CTC}}\end{aligned}$$

- χ^2 -analysis of lateral shower shape by looking at the energy sharing between towers on η :

$$\text{LSHR}$$

- χ^2 -analyses of lateral shower shapes on the strip (Z) and wire ($r \cdot \phi$) views by the CES:

$$\chi_{\text{strip}}^2, \chi_{\text{wire}}^2$$

3.1.3 Plug electron identification variables

- Hit occupancy of VTPC wire channels on the road between the vertex position and the cluster on the plug calorimeter:

$$f_{\text{hit}} = \frac{\# \text{ hit channels}}{\# \text{ total channels}}$$

- χ^2 -analysis of lateral shower shape by looking at the energy sharing between towers in the 3 by 3 segmentation on η - ϕ plane:

$$\chi_{3 \times 3}^2$$

3.1.4 Forward electron identification variables

In the forward region, the electron identification is not well established, because there is no useful tracking information. Therefore, the EM cluster in this region is examined only with the common variables.

3.2 Jet Identification

Jets are identified as clusters of energy in the calorimeter with a fixed cone algorithm [7], where the cone radius R_c is taken to be 0.7. Due to the non-linear response of the calorimeter for jets (including the effects of crack, magnetic field, and underlying event), the cluster energy has to be corrected to get a true parton momentum. It is found for example that the observed jet transverse energy $E_T^J = 10$ GeV corresponds roughly to the parton transverse momentum $p_T^{\text{parton}} = 15$ GeV/c [7]. Such a correction is made as a function of the jet energy and the position (η) on the calorimeter. The correction performance was checked out using dijet and direct γ samples [4].

3.3 Neutrino Identification

The presence of a neutrino is inferred by measuring the missing transverse energy (\cancel{E}_T) using the calorimeter. The missing transverse energy is defined as the magnitude of the vector sum of transverse energies over all the EM and HAD calorimeter towers in the region $|\eta| \leq 3.6$. Due to shower fluctuation and calorimeter response, the \cancel{E}_T resolution is $\sim 0.6/\sqrt{\Sigma E_T}$ where $\sqrt{\Sigma E_T}$ is the scalar sum of the transverse energy deposited in the entire calorimeter.

Due to the non-linearity of the calorimeter response, the missing energy has to also be corrected as well as for jets. The correction is made in conjunction with the jet energy correction. A proposed correction is

$$\vec{E}_T^\nu \equiv \vec{\cancel{E}}_T(\text{corrected}) = -\Sigma \vec{E}_T^e - \Sigma \vec{E}_T^J(\text{corrected}) - \alpha \cdot \vec{u},$$

where \vec{u} is the vector sum of transverse energies over all calorimeter towers for underlying event. The constant α is an overall correction of the non-linearity response of the calorimeter for the underlying event. The correction factor α is taken to minimize the width of the \cancel{E}_T distribution with the jet energy correction (see Section 3.2). Using the Z +jet sample, we obtained the correction factor to be 1.2.

The number 1.2 is slightly different from 1.4 used in W mass analysis [3]. The "underlying event" correction in the mass analysis is obtained from "no jet" sample, while our weak boson samples contain jets and the present algorithm makes an energy correction for jets in part with underlying event. This overcorrects the jet energy, so that the underlying event is undercorrected. In this analysis, we take 1.2 to be the correction factor for the underlying events.

4 CROSS SECTION RATIO FOR $W \rightarrow e \nu$ AND $Z \rightarrow e^+ e^-$

A test of the electroweak sector of the SM with the three generations can be made by a determination of Γ_W/Γ_Z , where Γ_W and Γ_Z depend on the top quark mass (M_{top}). An experimental determination of Γ_W/Γ_Z is equivalent to the measurement of the ratio R of $W \rightarrow e \nu$ to $Z \rightarrow e^+ e^-$ event rates [8]:

$$\begin{aligned} R &= \frac{\sigma_W \cdot B(W \rightarrow e \nu)}{\sigma_Z \cdot B(Z \rightarrow e^+ e^-)} \\ &= \frac{\sigma_W}{\sigma_Z} \cdot \frac{\Gamma(W \rightarrow e \nu)}{\Gamma(Z \rightarrow e^+ e^-)} \cdot \frac{\Gamma_Z}{\Gamma_W}, \end{aligned}$$

where $\Gamma(W \rightarrow e \nu)/\Gamma(Z \rightarrow e^+ e^-)$ and σ_W/σ_Z are theoretically calculable knowing the SM couplings, the parton distributions, and the weak boson masses. Therefore, the limit of the top quark mass (M_{top}) can be extracted. Furthermore, recent precision measurement of Γ_Z [9] allow us to measure Γ_W . The previous measurements on R have been reported by the UA1 and UA2 collaborations at $\sqrt{s} = 630$ GeV at the CERN $\bar{p}p$ Collider [10]. Here our measurement of R at $\sqrt{s} = 1.8$ TeV [11] is reported.

This test of the electroweak model is limited by the following uncertainties: (a) The theoretical uncertainty in the calculation of σ_W/σ_Z is mainly from the light quark distributions [12] and the charm quark distribution [13,14]. The uncertainty in R is estimated to be less than a few percent at $\sqrt{s} = 1.8$ TeV. (b) The experimental uncertainty in the measurement of R is dominated by the number of Z events. With an integrated luminosity of order 5 pb^{-1} , the CDF will be able to measure R to a precision better than 10%. Therefore, this is an expected limit from the present experimental result.

The W and Z events were selected from a common sample, "inclusive central electron events", with at least one well-measured, isolated, high E_T (≥ 20 GeV) electron in the central calorimeter. Loose cuts with high efficiency were then applied on the other lepton, a neutrino (W decay) or an electron (Z decay). For Z events, the invariant mass of the two electrons was required to be between 65 and 115 GeV/c². It was also required that there be no additional cluster with observed E_T greater than 10 GeV other than electron(s) in the event. This requirement reduces the systematic uncertainties and backgrounds in this measurement. There are 1828 events for the W sample and 192 events for the Z sample. The event selection cuts are summarized in Table 1.

Using these samples, the ratio R is experimentally obtained from

$$R = \frac{N_W}{N_Z} \cdot \frac{A_Z}{A_W} \cdot \frac{\epsilon_Z}{\epsilon_W},$$

where N_W (N_Z) is the number of W (or Z) events after the background subtraction, A_W (A_Z) is the acceptance of W (or Z) events with the fiducial cuts and the kinematic cut for electron(s), and ϵ_W (ϵ_Z) is the detection efficiency for neutrino (or electron) in W

(or Z) event. Detailed expression for ϵ_Z/ϵ_W is

$$\frac{\epsilon_Z}{\epsilon_W} = \frac{f_{CC} \cdot \epsilon_{C1} \cdot (2\epsilon_{C2} - \epsilon_{C1}) + f_{CP} \cdot \epsilon_{C1} \cdot \epsilon_P + f_{CF} \cdot \epsilon_{C1} \cdot \epsilon_F}{\epsilon_{C1} \cdot \epsilon_\nu}$$

Here f_{CC} (f_{CP} or f_{CF}) is a fraction of central (plug, or forward) Z 's, The parameters ϵ_{C1} , ϵ_{C2} , ϵ_P , ϵ_F , and ϵ_ν are the efficiencies for the first central electron (C1), second central electron (C2), plug electron (P), forward electron (F), and neutrino (ν). The central (plug or forward) Z means central-central (central-plug or central-forward) electrons in $Z \rightarrow e^+e^-$. The advantage of this technique is that the uncertainties in the integrated luminosity ($\sim 15\%$) and the efficiency ϵ_{C1} cancel in the ratio R.

The largest background in the W sample is from electroweak processes: (a) $W \rightarrow \tau \nu$, followed by $\tau \rightarrow e\nu\nu$, (b) $Z \rightarrow e^+e^-$, with the one electron undetected by the calorimeter, (c) $Z \rightarrow \tau^+\tau^-$, with subsequent decays into electrons and one of the two electrons undetected by the calorimeter. Using the ISAJET Monte Carlo [15] and the full CDF detector simulation program (CDFSIM), the background from those processes was estimated to be 83 ± 8 . The other background was estimated to be 18 ± 9 events from QCD jet production by studying the isolated and non-isolated electrons in the data. Those numbers are listed in Table 2.

On the other hand, the major background in the Z sample was estimated to be 5 ± 3 events from the jet production. For the background due to $Z \rightarrow \tau^+\tau^-$, no events were satisfied with the Z criteria in a ISAJET/CDFSIM simulation sample corresponding to 25 pb^{-1} . The background due to $W + 1\text{-jet}$, where the jet could fake the electron, was estimated to be 1 ± 1 event using PAPANENO Monte Carlo [16] and CDFSIM. These background estimates are also summarized in Table 2.

The acceptances (A_W and A_Z) and the event fractions (f 's) were estimated with a MC simulation which generates the bosons from the leading order diagram $q\bar{q} \rightarrow W(Z)$ using the various structure functions (MRSB, EHLQ, DO1) and a simple parametrization of the boson p_T spectrum. The generated events were processed through a simple detector simulation program with the measured energy resolutions and the fiducial volume of the CDF calorimeter. The efficiency for the neutrino was also estimated by the MC simulation. The efficiencies (ϵ 's) for electrons were obtained from the data. The results of these estimates are given in Table 2.

We also take into account two small corrections: (a) The "zero jet" requirement is expected to increase R by 0.8% [17], (b) Due to the Drell-Yan continuum under the Z mass peak, R must be decreased by 0.5%. Therefore, we multiply R by a factor 0.997. The number of R is obtained to be

$$R = \frac{\sigma_W \cdot B(W \rightarrow e \nu)}{\sigma_Z \cdot B(Z \rightarrow e^+e^-)} = 10.2 \pm 0.8 \text{ (stat.)} \pm 0.4 \text{ (sys.)}.$$

This is consistent with the SM prediction with heavy top quark ($M_{top} > M_W$) and $N_\nu = 3$ where a predicted value of R is 10.4 ± 0.1 [14]. Using the value of R, $\sin^2 \theta_W = 0.229$ [18], the predicted value of $\sigma_W/\sigma_Z = 3.23 \pm 0.03$ [14], and $\Gamma(W \rightarrow e\nu)/\Gamma(Z \rightarrow ee) =$

2.70 ± 0.02 [19], we extract $\Gamma_W/\Gamma_Z = 0.85 \pm 0.08$. Using the measured value of $\Gamma_Z = 2.57 \pm 0.07$ GeV [9], we find

$$\Gamma_W = 2.19 \pm 0.20 \text{ GeV.}$$

The SM prediction with $M_W = 80.0$ GeV/c², $\alpha_s = 0.13$, and $M_{top} \geq M_W - M_b$ is $\Gamma_W = 2.07$ GeV.

Figure 2 shows the top quark mass dependence of the ratio $\Gamma_W/\Gamma(W \rightarrow e\nu)$. Our measurement shows the ratio to be 9.8 ± 0.9 . This value excludes M_{top} below 41 (35) GeV/c² at the 90% (95%) confidence level. This is also consistent with a lower limit of 77 GeV/c² from the top quark searches in e +jets [20] and $e + \mu$ [21] channels.

5 W/Z + JETS

The production of weak bosons with hadronic jets at $\sqrt{s} = 1.8$ TeV is an important process to provide further tests of perturbative QCD at momentum transfer above the reach of the CERN $\bar{p}p$ Collider. The transverse momentum distribution of weak bosons are nice to test the QCD prediction [22,23]. More simply, the experimentally observed jet multiplicity “n” provides a good test of $\mathcal{O}(\alpha_s^n)$ calculation [24,25]. More importantly, a comparison of theoretical and experimental event rates will allow the identification of contributions from potential new physics source to the W, Z pair-production channels. For example, $t\bar{t} \rightarrow b\bar{b}W^+W^-$, where $M_{top} \geq M_W + M_b$. In fact the UA1 and UA2 experiments have actually reported several events ($W + 2$ -jet and $\cancel{E}_T + 2$ -jet events) which could be interpreted as WW, WZ , or ZZ with one boson decaying leptonically, one hadronically [26]. Therefore, the interesting quantities will be (1) p_T spectra of weak bosons (inclusive sample, $W + 1$ -jet and $W + 2$ -jet samples), (2) jet multiplicity, (3) invariant mass of two primary jets (M_{JJ}) in $W + 2$ (or 3) jets.

The W and Z samples for this analysis were selected from the common sample of events used in the R measurement and with the same strategy: A well-measured high E_T (≥ 20 GeV) electron in the central region and the other lepton (ν or e) with loose cuts. The selection cuts are given in Table 3. The requirements for electrons in this analysis were similar to those in the previous analysis, but were chosen with high efficiency for very high E_T ($\gtrsim 100$ GeV) electrons which are expected from high p_T boson events. For the neutrino, a cut for the missing E_T significance $S = \cancel{E}_T$ (*uncorrected*)/ $\sqrt{\Sigma E_T}$ was required in addition to \cancel{E}_T cut to prevent a mismeasurement of \cancel{E}_T by jet energy fluctuation since the events contain jets. The W selection was made by requiring the uncorrected transverse mass of electron and neutrino $M_T' = \sqrt{2 \cdot E_T^e \cdot \cancel{E}_T(\text{uncorrected}) \cdot (1 - \cos \phi_{e\nu})} \geq 40$ GeV. The Z selection was made with the invariant mass of two electrons between 75 and 105 GeV/c² where the second electron was required to be in the central or plug region. Those selection cuts leave 2,685 W events and 220 Z events. Figure 3(a) shows the distributions of $M_T = \sqrt{2 \cdot E_T^e \cdot E_T^\nu \cdot (1 - \cos \phi_{e\nu})}$ before and after the W selection cuts. In Fig. 3(a), the

peaks around W mass (Jacobian peak smeared by the calorimeter resolution) are seen for the inclusive W sample (dashed line) and W +jet sample (dotted line). Jets are identified as the observed jet $p_T \geq 10$ GeV/c in the region $|\eta| \leq 2.2$. We also show M_T distribution (solid line) of $e + \nu$ system without M_T' and S cuts, but with $E_T^\nu \geq 10$ GeV. Figure 3(b) shows the invariant mass distribution of dielectrons before the mass cuts in Z selection. We have estimated the background to be $\sim 4\%$ of those samples.

The p_T distribution for weak boson production is measured with a form

$$\frac{1}{\sigma} \frac{1}{p_T} \frac{d\sigma}{dp_T}.$$

In this form, some theoretical and experimental uncertainties (weak couplings, parton distribution dependence, luminosity *etc.*) tend to cancel in the ratio. The weak boson p_T is calculated as

$$\begin{aligned} \vec{p}_T^Z &= \vec{p}_T^{e^+} + \vec{p}_T^{e^-}, \\ \vec{p}_T^W &= \vec{p}_T^e + \vec{E}_T^\nu. \end{aligned}$$

The p_T distributions from the data and a theoretical prediction are shown in Figs. 4(a) and 4(b) for W and Z samples, respectively. The data points are corrected for the acceptance and efficiency. The solid curves are a particular theoretical calculation which includes a part of the complete $\mathcal{O}(\alpha_s^2)$ QCD calculation [22] using the MRSB parton distribution. For W sample, the background contamination is estimated to be increased to $\sim 20\%$ in the region $p_T^W \geq 80$ GeV/c. The correction for the spectrum smeared by the calorimeter resolution is estimated to be roughly 15% for $p_T^W \geq 80$ GeV/c. In the figure, such corrections are not applied yet because a careful study is underway. However, the agreement is still reasonable even if such size of correction is taken into account for the data points. A comparison of the data with a complete $\mathcal{O}(\alpha_s^2)$ calculation [23] for $d\sigma/dp_T$ is also underway. The result will be reported in the future.

A characterization of multi-jet events with weak bosons is simply made by looking at the jet multiplicity distributions. The fraction of the number of events with n -jets is defined as

$$f_n = \frac{\sigma_n}{\sum_{m=0} \sigma_m},$$

where σ_n is the weak boson production cross section with n -jets. We have an expected jet multiplicity from QCD calculations which are (i) Berends *et al.* (up to 3 jets) [24] and (ii) PAPAGENO (W +1-jet and W +2-jet) + CDFSIM. For (i), the theoretical counting of jets is made with $p_T^{\text{parton}} \geq 15$ GeV/c, which corresponds to 10 GeV in observed transverse energy of a cluster on the CDF calorimeter, and the angular separation of 2 partons $\Delta R \geq 0.7$ on η - ϕ plane. There is also a result on the independent calculation of the cross sections for weak boson with n -jets ($n = 0,1,2,3$) [25], which is completely in good agreement with the calculation by Berends *et al.* For (ii), we processed the

PAPAGENO events through ISAJET program (fragmentation, underlying event) since PAPAGENO is a parton-level event generator. Then the events were simulated with CDFSIM and selected with the same cuts as data. The MC events are normalized to data by ratio of luminosities for comparison. Such simulated samples are able to be compared to the data directly without any energy correction, because CDFSIM reproduces the non-linearity response of the calorimeter for jets and underlying event. These two predictions are shown with data in Fig. 5(a) for W sample. Figure 5(b) show only Z data, because theoretical prediction for Z is very similar to that for W . As seen in Fig. 5, both data and theoretical predictions are in good agreement. It is also seen that a very crude approximation $(\sigma_n/\sigma_0) \simeq (\sigma_1/\sigma_0)^n$ [27] works surprisingly well.

More interestingly, W +multi-jet data samples are compared with the MC events on p_T^W and M_{JJ} . Figures 6(a) and 6(b) show the distributions of uncorrected p_T^W for W +1-jet and W +2-jet data samples, respectively. The MC predictions (after normalization by the ratio of luminosities) are also presented. The agreements on the shape and the rate are reasonably good within the statistical errors of the data points. The distribution of M_{JJ} in the 2(or more)-jet events with the prediction is shown in Fig. 7. For the mass calculation, the jet energy correction was applied. The data is also in agreement with the MC.

Thus, from our preliminary work, weak boson data is expected as the QCD in weak boson p_T , jet multiplicity and the two jet invariant mass distributions.

6 CONCLUSIONS

Two tests have been made of electroweak sector and QCD of the Standard Model using a sample of weak bosons with subsequent decays into electron(s) in $\bar{p}p$ collisions at $\sqrt{s} = 1.8$ TeV. The measurement of the ratio $\sigma_W \cdot B(W \rightarrow e\nu)/\sigma_Z \cdot B(Z \rightarrow e^+e^-)$ provides a test of electroweak sector. The ratio is obtained to be 10.2 ± 0.8 (stat.) ± 0.4 (sys.). This is consistent with a theoretical prediction with $N_\nu = 3$ and $M_{top} \geq M_W$. From this result, we find $\Gamma_W = 2.19 \pm 0.20$ GeV and a lower limit of the top quark mass $M_{top} \geq 41$ (35) GeV/ c^2 at 90% (95%) CL. The QCD sector is tested by studying p_T distribution of weak bosons, multiplicity of associated jets (up to 3 jets), and the invariant mass spectrum of the associated 2 jets. The preliminary results are in good agreement with the QCD calculations.

ACKNOWLEDGEMENTS

This work would not have been possible without the dedication, skill and hard work of the Accelerator Division of Fermilab. We thank the staffs of our institutions for their many contributions to the construction of the detector. This work was supported by the U.S. Department of Energy, the National Science Foundation, Istituto Nazionale di Fisica Nucleare, the Ministry of Science, Culture and Education of Japan, and the A.P. Sloan Foundation.

APPENDICES

A The CDF Collaboration for the 1988-89 Run

F. Abe,⁽⁶⁾ D. Amidei,⁽⁴⁾ G. Apollinari,⁽¹¹⁾ M. Atac,⁽⁴⁾ P. Auchincloss,⁽¹⁴⁾ A. R. Baden,⁽⁶⁾
 A. Bamberger,⁽¹⁹⁾ A. Barbaro-Galtieri,⁽⁹⁾ V. E. Barnes,⁽¹²⁾ F. Bedeschi,⁽¹¹⁾
 S. Behrends,⁽²⁾ S. Belforte,⁽¹¹⁾ G. Bellettini,⁽¹¹⁾ J. Bellinger,⁽¹⁸⁾ J. Bensinger,⁽²⁾
 A. Beretvas,⁽⁴⁾ J. P. Berge,⁽⁴⁾ S. Bertolucci,⁽⁵⁾ S. Bhadra,⁽⁷⁾ M. Binkley,⁽⁴⁾ R. Blair,⁽¹⁾
 C. Blocker,⁽²⁾ A. W. Booth,⁽⁴⁾ G. Brandenburg,⁽⁶⁾ D. Brown,⁽⁶⁾ E. Buckley,⁽¹⁴⁾
 A. Byon,⁽¹²⁾ K. L. Byrum,⁽¹⁸⁾ C. Campagnari,⁽³⁾ M. Campbell,⁽³⁾ R. Carey,⁽⁶⁾
 W. Carithers,⁽⁹⁾ D. Carlsmith,⁽¹⁸⁾ J. T. Carroll,⁽⁴⁾ R. Cashmore,⁽¹⁹⁾ F. Cervelli,⁽¹¹⁾
 K. Chadwick,⁽⁴⁾ G. Chiarelli,⁽⁵⁾ W. Chinowsky,⁽⁹⁾ S. Cihangir,⁽⁴⁾ A. G. Clark,⁽⁴⁾
 D. Connor,⁽¹⁰⁾ M. Contreras,⁽²⁾ J. Cooper,⁽⁴⁾ M. Cordelli,⁽⁵⁾ D. Crane,⁽⁴⁾
 M. Curatolo,⁽⁵⁾ C. Day,⁽⁴⁾ S. Dell'Agnello,⁽¹¹⁾ M. Dell'Orso,⁽¹¹⁾ L. Demortier,⁽²⁾
 P. F. Derwent,⁽³⁾ T. Devlin,⁽¹⁴⁾ D. DiBitonto,⁽¹⁵⁾ R. B. Drucker,⁽⁹⁾ J. E. Elias,⁽⁴⁾
 R. Ely,⁽⁹⁾ S. Errede,⁽⁷⁾ B. Esposito,⁽⁵⁾ B. Flaugher,⁽¹⁴⁾ G. W. Foster,⁽⁴⁾ M. Franklin,⁽⁶⁾
 J. Freeman,⁽⁴⁾ H. Frisch,⁽³⁾ Y. Fukui,⁽⁸⁾ Y. Funayama,⁽¹⁶⁾ A. F. Garfinkel,⁽¹²⁾
 A. Gauthier,⁽⁷⁾ S. Geer,⁽⁶⁾ P. Giannetti,⁽¹¹⁾ N. Giokaris,⁽¹³⁾ P. Giromini,⁽⁵⁾
 L. Gladney,⁽¹⁰⁾ M. Gold,⁽⁹⁾ K. Goulios,⁽¹³⁾ H. Grassmann,⁽¹¹⁾ C. Grosso-Pilcher,⁽³⁾
 C. Haber,⁽⁹⁾ S. R. Hahn,⁽⁴⁾ R. Handler,⁽¹⁸⁾ K. Hara,⁽¹⁶⁾ R. M. Harris,⁽⁹⁾ J. Hauser,⁽³⁾
 T. Hessing,⁽¹⁵⁾ R. Hollebeek,⁽¹⁰⁾ L. Holloway,⁽⁷⁾ P. Hu,⁽¹⁴⁾ B. Hubbard,⁽⁹⁾
 B. T. Huffman,⁽¹²⁾ R. Hughes,⁽¹⁰⁾ P. Hurst,⁽⁷⁾ J. Huth,⁽⁴⁾ M. Incagli,⁽¹¹⁾ T. Ino,⁽¹⁶⁾
 H. Iso,⁽¹⁶⁾ H. Jensen,⁽⁴⁾ C. P. Jessop,⁽⁶⁾ R. P. Johnson,⁽⁴⁾ U. Joshi,⁽⁴⁾ R. W. Kadel,⁽⁴⁾
 T. Kamon,⁽¹⁵⁾ S. Kanda,⁽¹⁶⁾ D. A. Kardelis,⁽⁷⁾ I. Karliner,⁽⁷⁾ E. Kearns,⁽⁶⁾
 R. Kephart,⁽⁴⁾ P. Kesten,⁽²⁾ R. M. Keup,⁽⁷⁾ H. Keutelian,⁽⁷⁾ S. Kim,⁽¹⁶⁾ L. Kirsch,⁽²⁾
 K. Kondo,⁽¹⁶⁾ S. E. Kuhlmann,⁽¹⁾ E. Kuns,⁽¹⁴⁾ A. T. Laasanen,⁽¹²⁾ J. I. Lamoureux,⁽¹⁸⁾
 W. Li,⁽¹⁾ T. M. Liss,⁽⁷⁾ N. Lockyer,⁽¹⁰⁾ C. B. Luchini,⁽⁷⁾ P. Maas,⁽⁴⁾ M. Mangano,⁽¹¹⁾
 J. P. Marriner,⁽⁴⁾ R. Markeloff,⁽¹⁸⁾ L. A. Markosky,⁽¹⁸⁾ R. Mattingly,⁽²⁾ P. McIntyre,⁽¹⁵⁾
 A. Menzione,⁽¹¹⁾ T. Meyer,⁽¹⁵⁾ S. Mikamo,⁽⁸⁾ M. Miller,⁽³⁾ T. Mimashi,⁽¹⁶⁾ S. Miscetti,⁽⁵⁾
 M. Mishina,⁽⁸⁾ S. Miyashita,⁽¹⁶⁾ Y. Morita,⁽¹⁶⁾ S. Moulding,⁽²⁾ A. Mukherjee,⁽⁴⁾
 L. F. Nakae,⁽²⁾ I. Nakano,⁽¹⁶⁾ C. Nelson,⁽⁴⁾ C. Newman-Holmes,⁽⁴⁾ J. S. T. Ng,⁽⁶⁾
 M. Ninomiya,⁽¹⁶⁾ L. Nodulman,⁽¹⁾ S. Ogawa,⁽¹⁶⁾ R. Paoletti,⁽¹¹⁾ A. Para,⁽⁴⁾ E. Pare,⁽⁶⁾
 J. Patrick,⁽⁴⁾ T. J. Phillips,⁽⁶⁾ R. Plunkett,⁽⁴⁾ L. Pondrom,⁽¹⁸⁾ J. Proudfoot,⁽¹⁾
 G. Punzi,⁽¹¹⁾ D. Quarrie,⁽⁴⁾ K. Ragan,⁽¹⁰⁾ G. Redlinger,⁽³⁾ J. Rhoades,⁽¹⁸⁾ M. Roach,⁽¹⁷⁾
 F. Rimondi,⁽¹⁹⁾ L. Ristori,⁽¹¹⁾ T. Rohaly,⁽¹⁰⁾ A. Roodman,⁽³⁾ A. Sansoni,⁽⁵⁾
 R. D. Sard,⁽⁷⁾ A. Savoy-Navarro,⁽¹⁹⁾ V. Scarpine,⁽⁷⁾ P. Schlabach,⁽⁷⁾ E. E. Schmidt,⁽⁴⁾
 M. H. Schub,⁽¹²⁾ R. Schwitters,⁽⁶⁾ A. Scribano,⁽¹¹⁾ S. Segler,⁽⁴⁾ Y. Seiya,⁽¹⁶⁾
 M. Sekiguchi,⁽¹⁶⁾ P. Sestini,⁽¹¹⁾ M. Shapiro,⁽⁶⁾ M. Sheaff,⁽¹⁸⁾ M. Shochet,⁽³⁾ J. Siegrist,⁽⁹⁾
 P. Sinervo,⁽¹⁰⁾ J. Skarha,⁽¹⁸⁾ K. Sliwa,⁽¹⁷⁾ D. A. Smith,⁽¹¹⁾ F. D. Snider,⁽³⁾
 R. St. Denis,⁽⁶⁾ A. Stefanini,⁽¹¹⁾ R. L. Swartz, Jr.,⁽⁷⁾ M. Takano,⁽¹⁶⁾ K. Takikawa,⁽¹⁶⁾
 S. Tarem,⁽²⁾ D. Theriot,⁽⁴⁾ M. Timko,⁽¹⁵⁾ P. Tipton,⁽⁹⁾ S. Tkaczyk,⁽⁴⁾ A. Tollestrup,⁽⁴⁾

G. Tonelli,⁽¹¹⁾ J. Tonnison,⁽¹²⁾ W. Trischuk,⁽⁶⁾ Y. Tsay,⁽³⁾ F. Ukegawa,⁽¹⁶⁾
 D. Underwood,⁽¹⁾ R. Vidal,⁽⁴⁾ R. G. Wagner,⁽¹⁾ R. L. Wagner,⁽⁴⁾ J. Walsh,⁽¹⁰⁾
 T. Watts,⁽¹⁴⁾ R. Webb,⁽¹⁵⁾ C. Wendt,⁽¹⁸⁾ W. C. Wester, III,⁽⁹⁾ T. Westhusing,⁽¹¹⁾
 S. N. White,⁽¹³⁾ A. B. Wicklund,⁽¹⁾ H. H. Williams,⁽¹⁰⁾ B. L. Winer,⁽⁹⁾ A. Yagil,⁽⁴⁾
 A. Yamashita,⁽¹⁶⁾ K. Yasuoka,⁽¹⁶⁾ G. P. Yeh,⁽⁴⁾ J. Yoh,⁽⁴⁾ M. Yokoyama,⁽¹⁶⁾
 J. C. Yun,⁽⁴⁾ F. Zetti⁽¹¹⁾

⁽¹⁾ *Argonne National Laboratory, Argonne, Illinois 60439*

⁽²⁾ *Brandeis University, Waltham, Massachusetts 02254*

⁽³⁾ *University of Chicago, Chicago, Illinois 60637*

⁽⁴⁾ *Fermi National Accelerator Laboratory, Batavia, Illinois 60510*

⁽⁵⁾ *Laboratori Nazionali di Frascati, Istituto Nazionale di Fisica Nucleare, Frascati, Italy*

⁽⁶⁾ *Harvard University, Cambridge, Massachusetts 02138*

⁽⁷⁾ *University of Illinois, Urbana, Illinois 61801*

⁽⁸⁾ *National Laboratory for High Energy Physics (KEK), Tsukuba, Ibaraki 305, Japan*

⁽⁹⁾ *Lawrence Berkeley Laboratory, Berkeley, California 94720*

⁽¹⁰⁾ *University of Pennsylvania, Philadelphia, Pennsylvania 19104*

⁽¹¹⁾ *Istituto Nazionale di Fisica Nucleare, University and Scuola Normale Superiore of
 Pisa, I-56100 Pisa, Italy*

⁽¹²⁾ *Purdue University, West Lafayette, Indiana 47907*

⁽¹³⁾ *Rockefeller University, New York, New York 10021*

⁽¹⁴⁾ *Rutgers University, Piscataway, New Jersey 08854*

⁽¹⁵⁾ *Texas A&M University, College Station, Texas 77843*

⁽¹⁶⁾ *University of Tsukuba, Tsukuba, Ibaraki 305, Japan*

⁽¹⁷⁾ *Tufts University, Medford, Massachusetts 02155*

⁽¹⁸⁾ *University of Wisconsin, Madison, Wisconsin 53706*

⁽¹⁹⁾ *Visitor*

References

- [1] Abe, F. *et al.*, Nucl. Inst. and Meth. A271, 387 (1988).
- [2] Abe, F. *et al.*, Phys. Rev. Lett. 63, 720 (1989)
- [3] Phillips, T.J. (CDF Collaboration), these proceedings.
- [4] Bertolucci, S. (CDF Collaboration), these proceedings.
- [5] Abe, F. *et al.*, Phys. Rev. Lett. 62, 1005 (1989);
- [6] Proudfoot, J., Proceedings of the Workshop on Calorimetry for the Superconducting Supercollider, Tuscaloosa, Alabama, 12-17 March 1989; ANL-HEP-CP-89-40.
- [7] Abe, F., *et al.*, Phys. Rev. Lett. 62, 613 (1989).
- [8] Halzen, F. and Mursula, M., Phys. Rev. Lett. 51, 857 (1983); Hikasa, K., Phys. Rev. D29, 1939 (1984); Deshpande, G. *et al.*, Phys. Rev. Lett. 54, 1757 (1985).
- [9] Mark-II at SLC: Abrams, G. *et al.*, Phys. Rev. Lett. 63, 2173 (1989); ALEPH, DELPHI, L3, OPAL at LEP: to appear in Phys. Lett. B.
- [10] Albajar, C. *et al.*, Phys. Lett. 198B, 271 (1987); Ansari, R. *et al.*, Phys. Lett. 194B, 158 (1987).
- [11] Abe, F. *et al.*, to appear in Phys. Rev. Lett.
- [12] Martin, A.D., Stirling, W.J., and Roberts, R.G., Phys. Lett. B207, 205 (1988).
- [13] Berger, E.L. *et al.*, MAD/PH/400 (1988); ANL-HEP-PR-88-12 (1988).
- [14] Martin, A.D., Stirling, W.J., and Roberts, R.G., Phys. Lett. B228, 149 (1989).
- [15] Paige, F. and Protopopescu, S.D., ISAJET Monte Carlo V6.21, BNL Report No. BNL38034 (1986).
- [16] Hinchliffe, I., PAPAGENO (Parton-level event generator) Monte Carlo program.
- [17] Stirling, J., private communication.
- [18] Amaldi, U. *et al.*, Phys. Rev. D36, 1385 (1987).
- [19] See, for example, Hollik, W.F.L., DESY 88-188 (1988).
- [20] Abe, F. *et al.*, to appear in Phys. Rev. Lett.; Williams, H.H. (CDF Collaboration), these proceedings.

- [21] Abe, F. *et al.*, to appear in Phys. Rev. Lett.; Barbaro-Galtieri, A. (CDF Collaboration), these proceedings.
- [22] Bawa, A.C. and Stirling, W.J., Phys. Lett. B203, 172 (1988); Martin, A.D. *et al.*, Z.Phys. C42, 277 (1989).
- [23] Arnold, P.B., and Reno, M.H., FERMILAB-PUB-88/168-T (1988); ERRATA, FERMILAB-PUB-89/59-T (1989); to appear in Nucl. Phys. B.
- [24] Berends, F.A. *et al.*, University of Leiden Preprint, Preprint-89-0318 (1989)
- [25] Barger, V. *et al.*, MAD/PH/483 (1989); FSU-HEP-890420 (1989).
- [26] Denegri, D. (UA1 Collaboration), Proceedings in *Proton-Antiproton Collider Physics*, edited by K.Eggert, H.Faissner, and E.Radermacher (World Scientific, Singapore, 1987); Loucatos, S. (UA2 Collaboration), *ibid.*
- [27] Ellis, S.D., Kleiss, R., and Stirling, W.J., Phys. Lett. 154B, 435 (1985).

Table 1 Event Selection for $\sigma_W \cdot B(W \rightarrow e\nu) / \sigma_Z \cdot B(Z \rightarrow e^+e^-)$
Analysis

- Primary event section ($|Z_{\text{vertex}}| \leq 60$ cm)
- Central electron ($|\eta| \leq 1.0$)
 - $E_T \geq 20$ GeV
 - $I \leq 0.1$
 - HAD/EM ≤ 0.05
 - $\Delta(r \cdot \phi) \leq 2.5$ cm, $\Delta Z \leq 3.0$ cm
 - $0.5 \leq E/p \leq 2.0$
 - LSHR ≤ 0.2
 - $\chi_{\text{strip}}^2 \leq 15$
 - Fiducial cuts (cracks, bad towers)
- W 's
 - Central electron
 - $E_T \geq 20$ GeV
 - No additional cluster with observed $E_T \geq 10$ GeV other than the electron
- Z 's
 - Central electron
 - 2nd electron (in central, plug, and forward) with
 - $E_T \geq 10$ GeV
 - $I \leq 0.2$
 - HAD/EM ≤ 0.1
 - $0.5 \leq E/p \leq 2.0$ if central electron; $\chi_{3 \times 3}^2 \leq 20$ if plug electron
 - Fiducial cuts (cracks, bad towers)
 - $65 \text{ GeV}/c^2 \leq M_Z \leq 115 \text{ GeV}/c^2$
 - No additional cluster with observed $E_T \geq 10$ GeV other than the electrons

Table 2 Summary of $\sigma_W \cdot B(W \rightarrow e\nu) / \sigma_Z \cdot B(Z \rightarrow e^+e^-)$
Analysis

Quantity	W Events	Z Events
$N_{observed}$	1828	192
<u>Background</u>		
$W \rightarrow \tau \nu$	67 ± 6	—
$Z \rightarrow e e$	12 ± 5	—
$Z \rightarrow \tau \tau$	4 ± 1	0.0
W + EM jet	—	1 ± 1
QCD $b\bar{b}$	18 ± 9	5 ± 3
Total background	101 ± 12	6 ± 3
N_W or N_Z	$1727 \pm 43 \pm 10$	$186 \pm 14 \pm 3$
<u>Acceptance</u>		
A_W or A_Z	0.351 ± 0.0011	0.374 ± 0.0011
<u>Efficiency</u>		
f_{CC}	—	0.39
f_{CP}	—	0.47
f_{CF}	—	0.14
ϵ_{C1}	0.86 ± 0.03	0.86 ± 0.03
ϵ_{C2}	—	0.96 ± 0.02
ϵ_P	—	0.96 ± 0.03
ϵ_F	—	0.97 ± 0.03
ϵ_ν	0.965 ± 0.005	—
ϵ_W or ϵ_Z	0.83 ± 0.03	0.88 ± 0.03

Table 3 Event Selection for $W/Z + n$ -jet Analysis

- Primary event section ($|Z_{\text{vertex}}| \leq 60$ cm)
- Central electron ($|\eta| \leq 1.0$)
 - $E_T \geq 20$ GeV
 - $I \leq 0.1$
 - $\text{HAD}/\text{EM} \leq 0.055 + 0.045 \times \text{EM}/100$ (0.1 at 100 GeV)
 - $\Delta(r \cdot \phi) \leq 1.5$ cm, $\Delta Z \leq 3.0$ cm
 - $E/p \leq 1.5$ or $p_T \geq 20$ GeV/c
 - $\text{LSHR} \leq 0.2$
 - Fiducial cuts (cracks, bad towers)
- W 's
 - Central electron
 - $E_T \geq 20$ GeV
 - $\cancel{E}_T / \sqrt{\Sigma E_T} \geq 2.4$
 - $M_T' \geq 40$ GeV, where $M_T' = \sqrt{2 \cdot E_T^e \cdot \cancel{E}_T \cdot (1 - \cos \phi_{e\nu'})}$
 - Note above \cancel{E}_T is uncorrected value
- Z 's
 - Central electron
 - 2nd electron (in central or plug region)
 - $E_T \geq 10$ GeV
 - $I \leq 0.2$
 - $\text{HAD}/\text{EM} \leq 0.055 + 0.045 \times \text{EM}/100$ (0.1 at 100 GeV)
 - $\text{LSHR} \leq 0.2$ (central); $\chi_{3 \times 3}^2 \leq 20$, $f_{\text{hit}} \geq 0.5$ (plug)
 - Fiducial cuts (cracks, bad towers)
 - $75 \text{ GeV}/c^2 \leq M_Z \leq 105 \text{ GeV}/c^2$
- Jets
 - Uncorrected $p_T \geq 10$ GeV/c
 - $|\eta_{\text{jet}}| \leq 2.2$

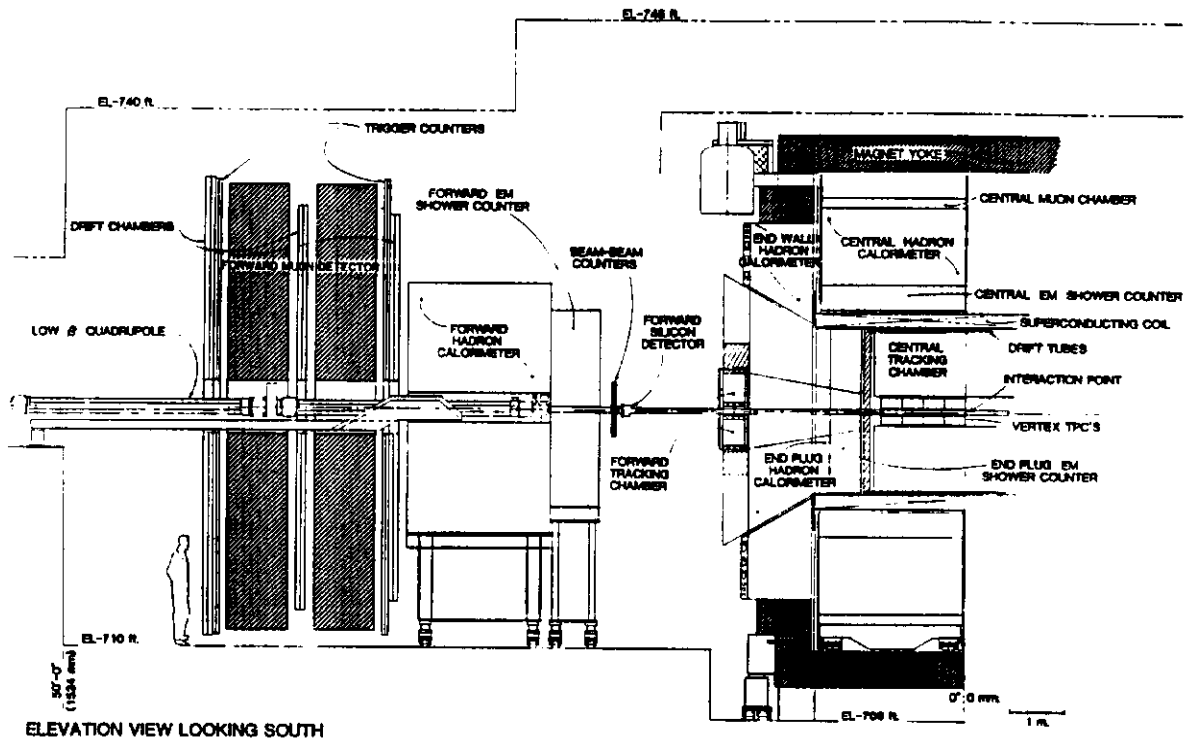


Figure 1: A cut-away view through the forward half of CDF. The detector is forward-backward symmetric about the interaction point.

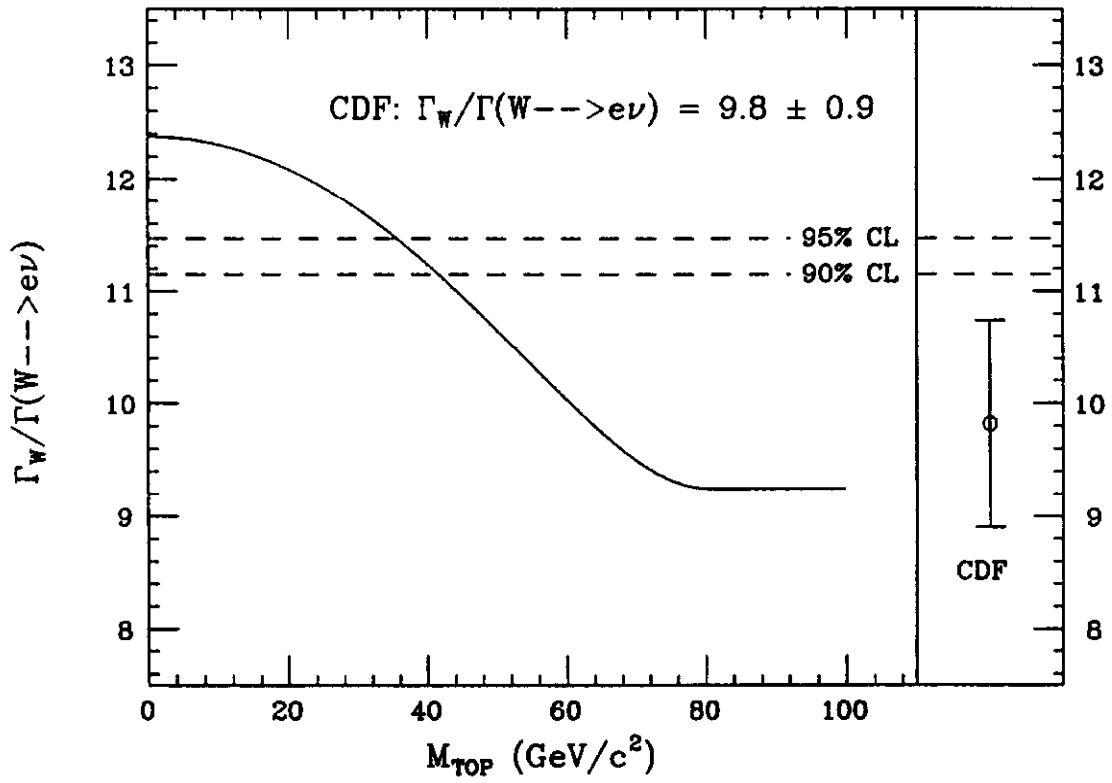


Figure 2: $\Gamma_W/\Gamma(W \rightarrow e \nu)$ vs M_{top} . The solid curve is the expectation from the SM with $M_W = 80.0 \text{ GeV}/c^2$, $\alpha_s = 0.13$, and $N_\nu = 3$. The data point and 90% (95%) CL lines are also shown with the measured value.

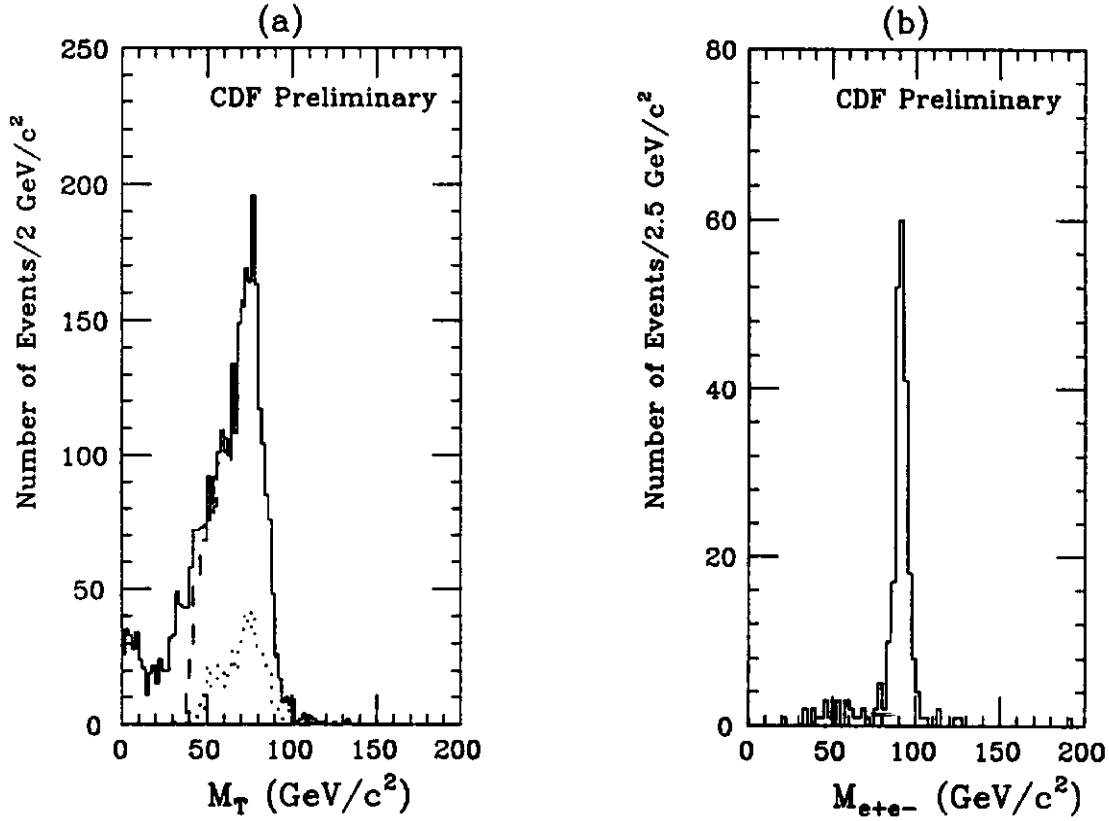


Figure 3: (a) The transverse mass (M_T) distributions for $W \rightarrow e\nu$ events before and after the W selection cuts. The solid line is for the sample with $E_T^e \geq 20$ GeV for a well-measured central electron and $E_T^\nu \geq 10$ GeV. The dashed line is for W sample (see the text for the selection cuts). The dotted line is for W +jet sample with uncorrected $p_T^J \geq 10$ GeV/c in $|\eta| \geq 2.2$. (b) The invariant mass (M_{ee}) distribution for $Z \rightarrow e^+e^-$ events before the mass cuts. See the text for the Z selection.

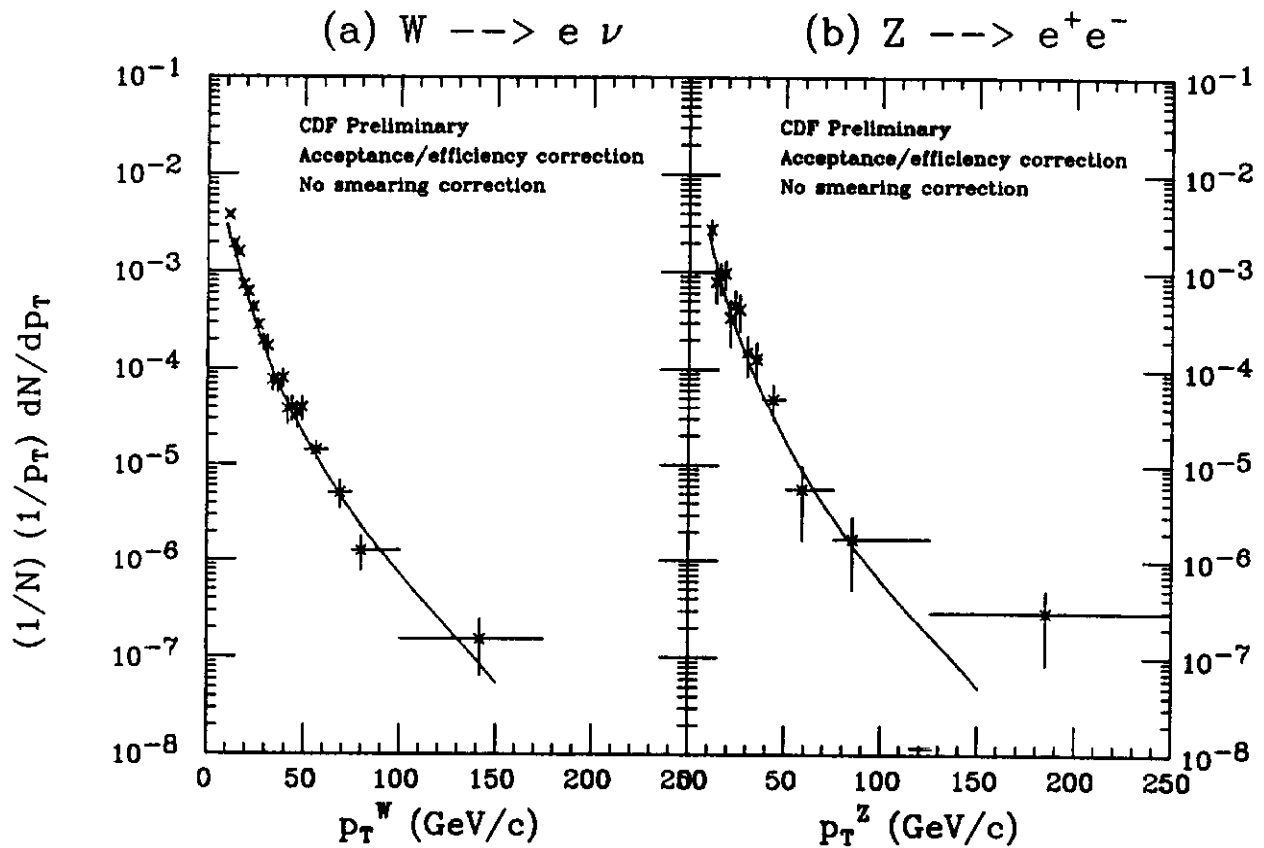


Figure 4: Inclusive p_T spectra for (a) W and (b) Z events. The correction for the spectrum smeared by the calorimeter resolution is not applied yet (see the text in detail). A theoretical prediction [22] is also shown with solid line.

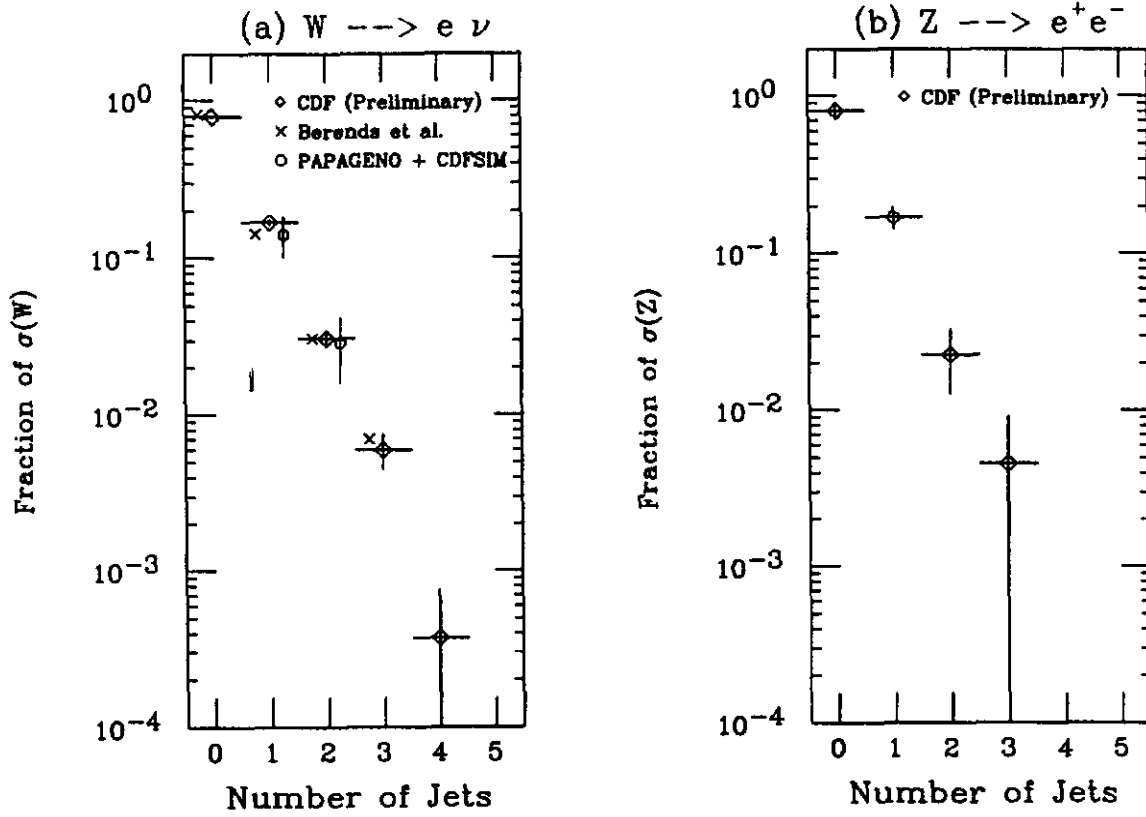


Figure 5: Jet multiplicity distributions for (a) W and (b) Z samples. Two theoretical calculations for W are also shown: One is by Berends *et al.* [24], other by PAPANENO+CDFSIM. Note the prediction for Z is very similar to that for W .

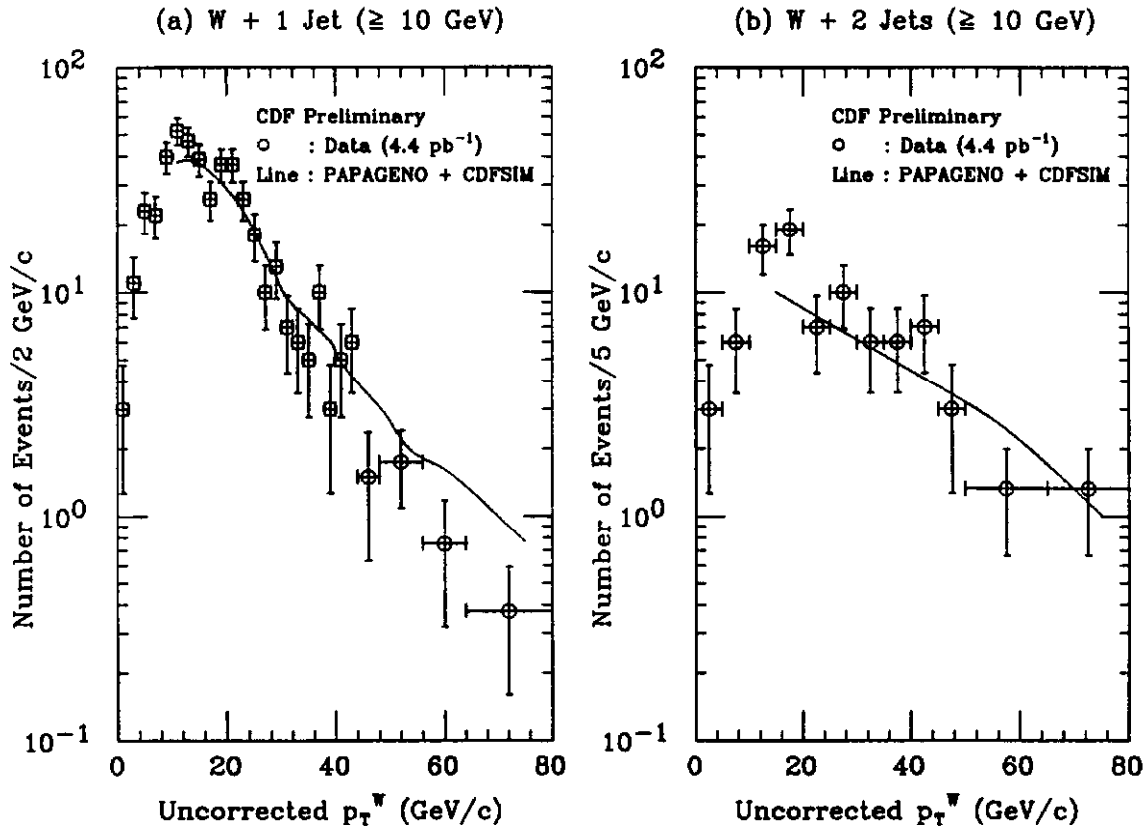


Figure 6: (a) $W p_T$ spectrum for $W + 1$ -jet sample. (b) $W p_T$ spectrum for $W + 2$ -jet sample. The predictions are shown with solid curve from PAPAGENO + CDFSIM with normalization by the ratio of luminosities. Note p_T^W is uncorrected value on the missing E_T . See the text in detail.

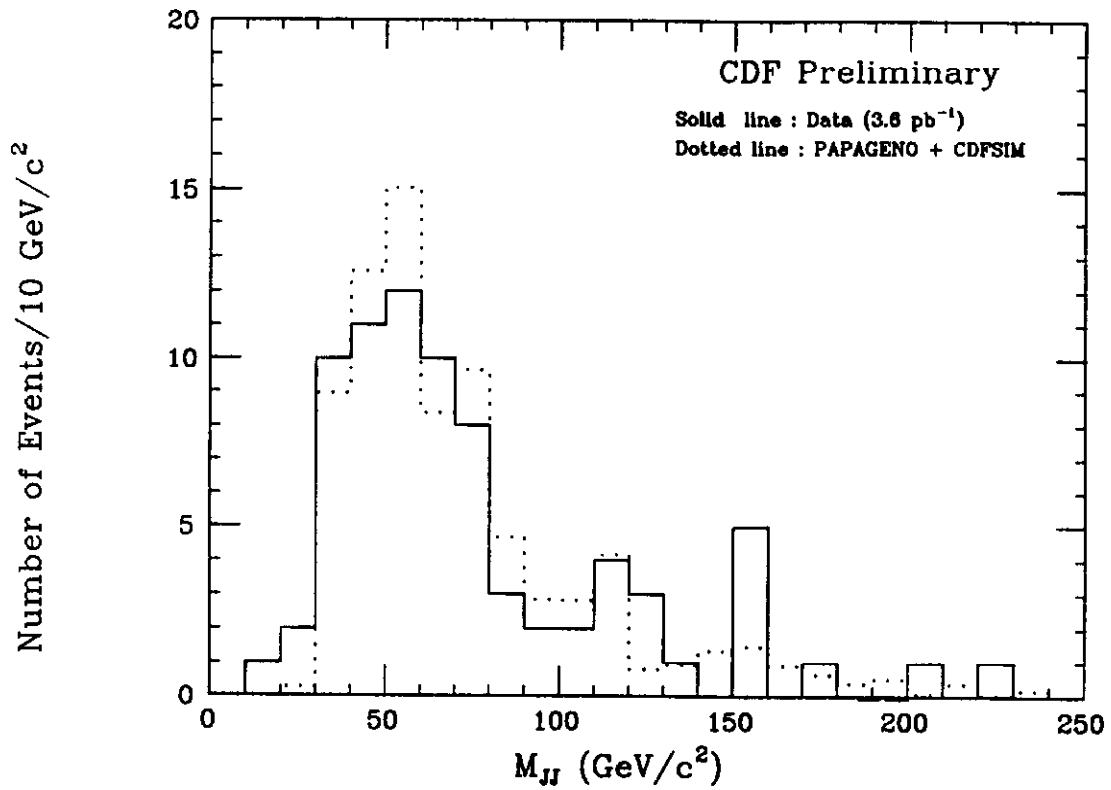


Figure 7: The invariant mass distribution of two jets (M_{JJ}) for $W + n$ ($n \geq 2$) jets sample. Solid line is the prediction by PAPANENO + CDFSIM MC simulation with normalization by equal area of the distribution.